KamLAND's precision neutrino oscillation measurements

Decowski, M.P.; KamLAND Collaboration

DOI
10.1016/j.nuclphysb.2016.04.014
Publication date
2016
Document Version
Final published version
Published in
Nuclear Physics B

Available online at www.sciencedirect.com

ScienceDirect

Nuclear Physics B 908 (2016) 52–61

NUCLEAR PHYSICS B

www.elsevier.com/locate/nuclphysb

KamLAND's precision neutrino oscillation measurements

M.P. Decowski for the KamLAND Collaboration

Nikhef and the University of Amsterdam, Science Park, Amsterdam, The Netherlands

Received 22 February 2016; received in revised form 6 April 2016; accepted 7 April 2016

Available online 13 April 2016

Editor: Tommy Ohlsson

Abstract

The KamLAND experiment started operation in the Spring of 2002 and is operational to this day. The experiment observes signals from electron antineutrinos from distant nuclear reactors. The program, spanning more than a decade, allowed the determination of LMA-MSW as the solution to the solar neutrino transformation results (under the assumption of *CPT* invariance) and the measurement of various neutrino oscillation parameters. In particular, the solar mass-splitting Δm^2_{21} was determined to high precision. Besides the study of neutrino oscillation, KamLAND started the investigation of geologically produced antineutrinos (geo-$\bar{\nu}_e$). The collaboration also reported on a variety of other topics related to particle and astroparticle physics.

1. Introduction

Japan began operation of its first commercial nuclear power plant in the mid-1960s. The country invested heavily in nuclear reactors to generate electricity in the subsequent decades and by the year 2000 about 50 nuclear reactors provided 30% of the country's electricity. Besides producing electricity, nuclear reactors also emit electron antineutrinos ($\bar{\nu}_e$) isotropically in the decay of neutron-rich radioactive products of the fission process. These well-defined sources of $\bar{\nu}_e$'s give the opportunity to study neutrino properties.

E-mail address: decowski@nikhef.nl (M.P. Decowski).

http://dx.doi.org/10.1016/j.nuclphysb.2016.04.014

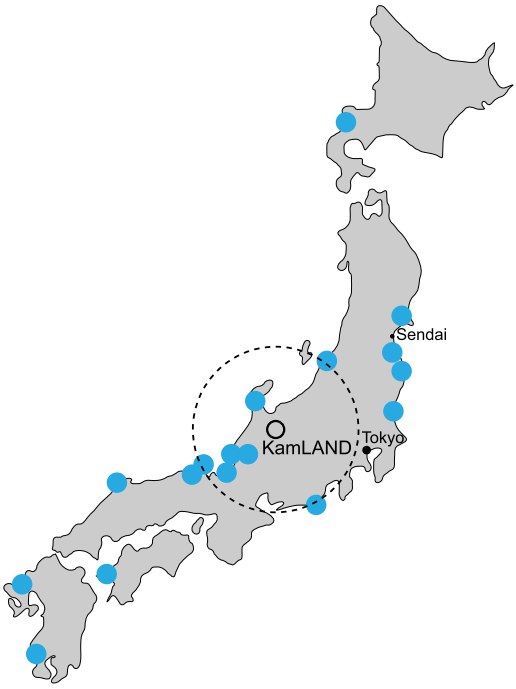

Fig. 1. The KamLAND experiment is located in the Kamioka Mine. The experiment is surrounded by more than 50 nuclear reactors at various commercial Nuclear Power Plants (blue dots). Most Nuclear Power Plants operate multiple reactors. The flux-weighted average distance of the reactors to KamLAND is ∼180 km (dashed circle). (For interpretation of the references to color in this figure legend, the reader is referred to the web version of this article.)

The Kamioka Liquid Scintillator Anti-Neutrino Detector (KamLAND) experiment was proposed in 1994 [1,2] and was approved by the Japanese government in 1997. In the following years, groups from Japan and the U.S. built the experiment in the old Kamiokande [3] cavity in the Kamioka Mine (Gifu Prefecture, Japan). The initial goals of KamLAND were the search for neutrino oscillation, the first observation of neutrinos originating from radioactive decays in the Earth's mantle (so-called geo-neutrinos) and the possible detection of galactic Supernovae. The KamLAND experiment was completed in early 2002. After a brief detector commissioning phase, regular scientific data recording started on March 9, 2002.

The location of the Kamioka Mine in relation to the Japanese nuclear power reactors provided a flux-weighted average distance of ∼180 km. About 80% of the neutrino flux in 2002 came from 26 reactors within a distance range of 138–214 km, see Fig. 1. The 180 km baseline, together with the emitted $\bar{\nu}_e$ spectrum peaking at ∼4 MeV, made KamLAND primarily sensitive to the neutrino oscillation solutions of the 'solar neutrino problem' for solar mass-splitting values of $\Delta m^2_{21} > 10^{-5}$ eV^2.

This review summarizes the KamLAND results obtained in five neutrino-oscillation-related data-releases between 2002 and 2013 [4–8].

2. The KamLAND detector

The KamLAND detector is located in the Kamioka Mine under Mount Ikenoyama at a depth of ∼2700 m water-equivalent. The primary volume consists of 1 kton of ultra-pure liquid scin-

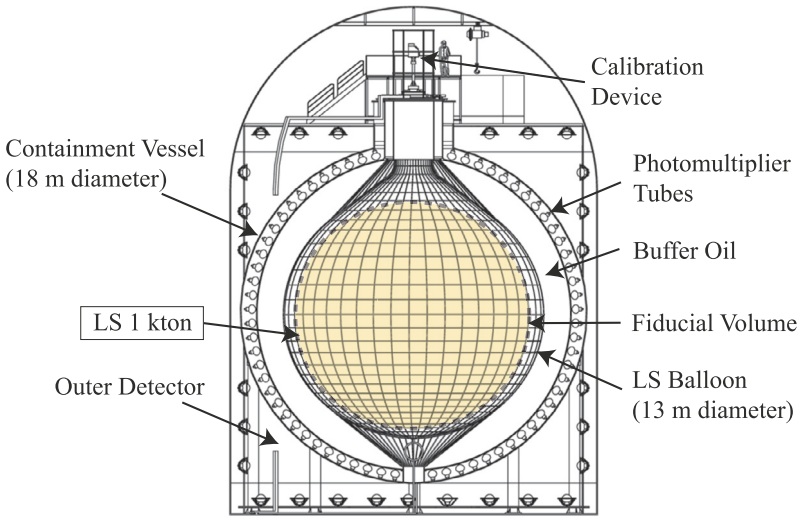

Fig. 2. Schematic diagram of the KamLAND detector. The primary target volume of the inner detector consists of ∼1 kton of ultra-pure liquid scintillator (LS). The inner detector is shielded by a water-Cherenkov outer detector.

tillator (LS), which provides the neutrino interaction target, see Fig. 2. The LS consists of 80% dodecane and 20% pseudocumene by volume and (1.36 ± 0.03) g/liter PPO[1] as a fluor. The LS is contained in a 13-m-diameter spherical balloon made of 135-μm-thick transparent nylon/EVOH[2] composite film. The balloon is suspended in non-scintillating purified mineral oil (so-called buffer oil). The inner detector (ID) is inside an 18-m-diameter stainless steel spherical tank. Bolted to the inside of the tank are 1325 fast 20-inch-diameter photo multiplier tubes (PMTs), masked to 17-inch diameter, and 554 20-inch-diameter PMTs viewing the inside volume of the ID. The PMT coverage is 34%. The ID is surrounded by a 3.2 kton water-Cherenkov outer detector (OD) that serves as a cosmic-ray muon veto and provides additional shielding from external sources of radioactivity.

KamLAND is sensitive to $\bar{\nu}_e$'s through the inverse β-decay reaction, $\bar{\nu}_e + p \rightarrow e^+ + n$, with a reaction threshold of 1.8 MeV. This process has a delayed coincidence event pair signature which provides strong radioactive background suppression. The positron carries most of the energy of the incoming antineutrino from the reaction and is annihilated quickly, providing a prompt event. An approximation of the incident $\bar{\nu}_e$ energy is given by $E_{\bar{\nu}_e} \simeq E_p + \overline{E}_n + 0.8$ MeV, where E_p, the prompt energy, is the sum of the positron kinetic and annihilation energies. $\overline{E}_n$ is the average neutron recoil energy and is of order tens of keV. The delayed event of the delayed coincidence event pair is produced by the capture-γ when the neutron captures on either a proton or a ^{12}C nucleus in the LS, with a mean capture time of 207.5 ± 2.8 μs [9].

The event vertex and energy reconstruction algorithms are based on the timing and charge distribution of scintillation photons recorded by the 17-inch and 20-inch PMTs. These algorithms were tuned with a wide variety of radioactive sources over the lifetime of the experiment. The sources that have been deployed are: ^{60}Co, ^{65}Zn, ^{68}Ge, ^{137}Cs, ^{203}Hg, ^{210}Po^{13}C, ^{241}Am^{9}Be,

[1] 2,5-diphenyloxazole.
[2] Ethylene vinyl alcohol copolymer.

spanning a variety of energies and particles. Deployments were routinely done through the central calibration system at the top of the detector [10], see Fig. 2, but a full-volume campaign was also performed [11]. The vertex resolution is $\sim$12 cm/$\sqrt{E(\mathrm{MeV})}$, and the energy resolution, using both the 17-inch and 20-inch PMTs, is 6.4%/$\sqrt{E(\mathrm{MeV})}$. The conversion between the deposited energy and KamLAND's prompt energy scale is non-linear and particle-dependent. We use a model that includes Birk's quenching and Cherenkov-light emission with parameters constrained by the calibration data to make the conversion. The systematic uncertainties in this model, estimated at 1.8%, is the largest contribution to the uncertainty on Δm^2_{21}.

The event vertex information is used in order to limit the search for candidate $\bar{\nu}_e$ events to a central fiducial volume, where the signal-to-background is estimated to be highest. The initial publication [4] used 5.0 m as the radius defining the spherical fiducial volume in the KamLAND detector, this was later expanded to 5.5 m [12]. Radioactive backgrounds near the surface of the balloon can cause accidental backgrounds (see Section 4). As the understanding of the backgrounds on the balloon grew, it became possible to model them and increase the fiducial-volume-radius to 6.0 m [6] through the use of a likelihood discriminator to suppress these accidental backgrounds.

The KamLAND detector was modified in September 2011 to accommodate the KamLAND-Zen neutrinoless double beta-decay experiment [13]. The initial phase of KamLAND-Zen used about 300 kg of ^{136}Xe loaded into 13 tons of liquid scintillator, all contained in a 3-m-diameter balloon at the center of the detector. The KamLAND and KamLAND-Zen phases continue to coexist.

3. Reactor signal

To calculate the expected $\bar{\nu}_e$-signal from nuclear reactors, the collaboration uses detailed reactor operation records, which are provided by a consortium of Japanese electric power companies. These include the thermal power variation as well as refueling and fuel rearrangement data from all Japanese commercial reactors. The absolute thermal power, used to normalize the fission rates, is measured to within 2% for each reactor [14]. The data points are typically provided weekly, or more often, with a period of 1 h or even 10 min when the operating parameters vary more quickly. This information, combined with publicly available world reactor data, is used to calculate the instantaneous fission rates using a reactor model. Only four fission isotopes contribute significantly to the $\bar{\nu}_e$ spectrum. The ratios of the fission yields averaged over the entire livetime period up to the latest data-release in 2013, are (0.567 : 0.078 : 0.298 : 0.057) for (^{235}U : ^{238}U : ^{239}Pu : ^{241}Pu). Although their contribution is small, long-lived, out-of-equilibrium fission products ^{90}Sr, ^{106}Ru and ^{144}Ce are also included in the calculations. The emitted $\bar{\nu}_e$ energy spectrum is calculated using $\bar{\nu}_e$ spectra from [15,16]. Neutrino oscillation effects distort the $\bar{\nu}_e$ spectrum as the $\bar{\nu}_e$'s travel from the reactors to KamLAND. Observation of this effect is therefore direct evidence for neutrino oscillation. The time evolution of the expected and observed detection rates at KamLAND is shown in Fig. 3.

When the neutrino fluxes were highest, roughly 95% of the $\bar{\nu}_e$ flux at KamLAND came from Japanese power reactors, $\sim$3.5% came from Korean reactors and about 1% came from reactors around the world. The total $\bar{\nu}_e$ flux and these ratios changed dramatically following the Fukushima nuclear accident in March 2011. All Japanese nuclear reactors were shutdown by September 2013 due to a review of nuclear safety. The absence of a $\bar{\nu}_e$-signal from Japanese reactors at KamLAND lasted until August 2015, when one of the reactors was put back into operation.

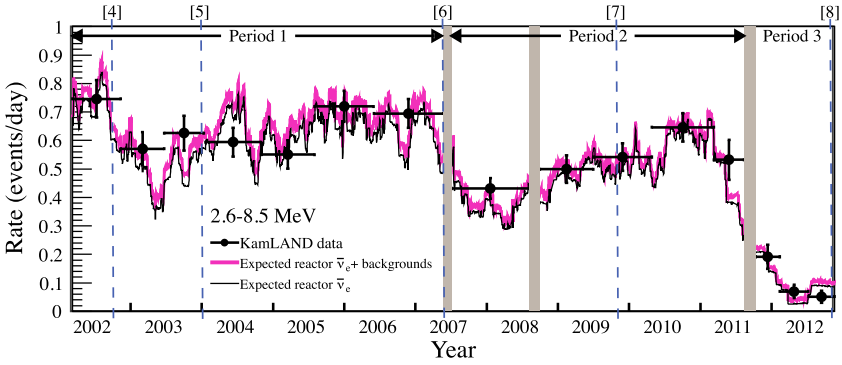

Fig. 3. Time evolution of expected and observed rates at KamLAND for electron antineutrinos for prompt energies above 2.6 MeV. The data points indicate the average observed $\bar{\nu}_e$ rate as measured by KamLAND. The black line gives the expected rate, based on detailed operational records of nuclear reactors, including effects due to neutrino oscillation. The colored line gives the expected $\bar{\nu}_e$ rate at KamLAND, including the reactor signal and backgrounds. The eleven-year data-taking span has been subdivided into three periods corresponding to distinct phases of the KamLAND detector. The end-periods of the five data-releases (Ref. indicated at the top) are also shown (dashed vertical lines). (For interpretation of the references to color in this figure, the reader is referred to the web version of this article.)

4. Backgrounds

The delayed coincidence event pair technique to identify the $\bar{\nu}_e$-candidates through the inverse β-decay reaction, described in Section 2, strongly suppresses backgrounds from radioactivity. Nevertheless, a number of backgrounds are important in the analysis of KamLAND data.

The rate of accidental coincidences increases in the outer region of the fiducial volume. This background can be accurately estimated through the pairing of random single events. Below 2.6 MeV prompt energy, the reactor-$\bar{\nu}_e$ background is expected to be dominated by geologically produced antineutrinos or geo-$\bar{\nu}_e$. These are antineutrinos from the decay chains of ^{238}U and ^{232}Th in the Earth. While they are a background to KamLAND's neutrino oscillation measurements, they are also an interesting signal in their own right, providing a glimpse into the Earth's interior [17,18]. The geo-$\bar{\nu}_e$ background can be avoided by requiring a 2.6 MeV E_p-threshold for the neutrino oscillation studies.

One unexpected background was the discovery of a correlated background due to $^{13}\mathrm{C}(\alpha,\mathrm{n})^{16}\mathrm{O}$ reactions from α-decay of ^{210}Po, a daughter of ^{222}Rn introduced into the LS during construction. This was the main background until May 2007 (Period 1 in Fig. 3), when the collaboration embarked on a liquid scintillator purification campaign. The purification campaign reduced the $^{13}\mathrm{C}(\alpha,\mathrm{n})^{16}\mathrm{O}$ decays by a factor of $\sim$20, effectively removing the background in subsequent years.

Above 2.6 MeV, neutrons, atmospheric neutrinos and long-lived delayed-neutron β-emitters are sources of correlated backgrounds. Roughly 3000 neutrons per kton-day are produced through spallation processes, but these are eliminated by a 2 msec full-volume veto after a passing muon. The remaining fast neutrons come from muons missed by the OD or interacting in the rock just outside of it, but these are also suppressed by several layers of absorbers. The surviving neutrons can scatter and capture in the LS, mimicking the $\bar{\nu}_e$ signal. We also expect backgrounds from atmospheric neutrinos, but their number is relatively small. Finally, the cosmogenically produced delayed-neutron β-emitters ^{8}He ($T_{1/2} = 119$ msec) and ^{9}Li ($T_{1/2} = 178$ msec) also

contribute to the background. They are predominately produced in so-called "showering muons", muons that deposit a large amount of energy in the liquid scintillator. We suppress them by requiring a 2-sec veto of the entire volume after a showering muon or a 2-sec veto of a 3-m-radius volume around a muon track. See Ref. [9] for a detailed discussion of the cosmogenically produced backgrounds in KamLAND.

5. Results

The first KamLAND results were released in December 2002 [4], shortly after the first SNO measurement of solar neutrino flavor transformation [19]. The initial KamLAND results showed evidence for reactor antineutrino disappearance. Assuming *CPT* invariance, this result eliminated all but the LMA-MSW oscillation solution as the explanation of the solar neutrino flavor transformation. In the subsequent decade, KamLAND was able to report on more and more precise neutrino oscillation parameters in the solar sector.

5.1. Neutrino oscillation results

Details of the $\bar{\nu}_e$-candidate selection cuts can be found elsewhere [4–8]. The most recent data release of 2013 identified 2611 candidate $\bar{\nu}_e$'s, with an expected background (excluding geo-$\bar{\nu}_e$) of 364.1 ± 30.5 events.

Fig. 4 shows the prompt energy $\bar{\nu}_e$-candidate spectra separately for the three periods when the KamLAND detector was in distinct running conditions. As discussed in Section 4, Period 1 was dominated by the significant background from $^{13}\mathrm{C}(\alpha, \mathrm{n})^{16}\mathrm{O}$, which was substantially reduced during a purification campaign starting in 2007. Period 3 starts after the inner-balloon for the KamLAND-Zen [13] experiment was installed in September 2011. This period coincides with the low reactor neutrino flux following the Fukushima nuclear accident in March 2011.

The energies of reactor antineutrinos and the average baseline of ∼180 km allowed KamLAND to analyze the first years of data in a two-neutrino framework (i.e., assuming $\theta_{13} = 0$). By the time of the data-release in 2010, the data-set was sufficiently large to extend this to a three-neutrino analysis with Earth-matter effects. This in turned allowed not only the measurement of Δm^2_{21} and θ_{12}, but also the possibility to constrain θ_{13}.

Fig. 5 shows the evolution of the allowed solar neutrino oscillation parameter regions, from 2002 up until the latest KamLAND data-release in 2013. The first data in 2002 [4] allowed, under the assumption of *CPT* invariance, to restrict the solar neutrino oscillation parameter space to $\Delta m^2_{21} > \sim 10^{-5}$ eV^2. However, several regions of Δm^2_{21} were still allowed at 95% C.L. (blue shaded regions in Fig. 5). The 2004 data-release [5] reduced the allowed parameter space to three distinct Δm^2_{21} parameter regions at 95% C.L. By 2008 the shape-distortion effects in the reactor spectrum allowed to shrink Δm^2_{21} to one parameter region. Table 1 lists the 2013 KamLAND neutrino oscillation parameter results under various combinations of experimental data. Δm^2_{21} is now one of the most precisely determined neutrino oscillation parameters. The allowed region contours in the panels in Fig. 5 also show the complementarity between the KamLAND results and the solar results: the solar results allow a precision measurement of θ_{12}, while KamLAND provides a measurement of Δm^2_{21}.

Finally, Fig. 6 provides an illustration of the oscillatory nature of the signal measured by KamLAND. The data points in Fig. 6 are the ratio of the observed reactor $\bar{\nu}_e$ spectrum to that expected in the case of no-oscillation shown as a function of $L_0/E_{\bar{\nu}_e}$, where L_0 is the flux-

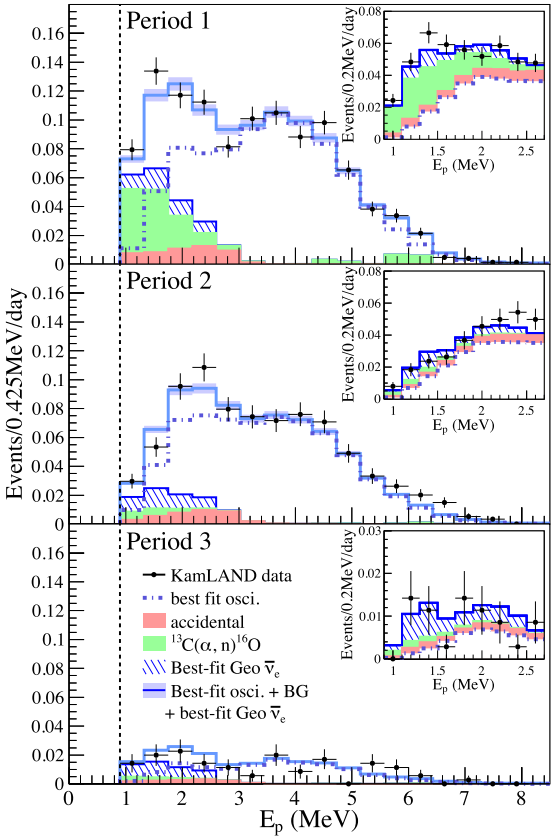

Fig. 4. Prompt energy spectrum of $\bar{\nu}_e$-candidate events for each data taking period (see Fig. 3), the inset shows the prompt spectrum with a finer binning for low-energy events. KamLAND suffered from a large radioactive background in the first period of data taking. This was significantly reduced after a purification campaign (Period 2). Period 3 is after the installation of an inner-balloon for the KamLAND-Zen experiment in September 2011. It coincides with a low reactor neutrino flux period following the Fukushima reactor accident. Figure adapted from [8].

Table 1
Summary of the fit values for Δm^2_{21}, $\tan^2\theta_{12}$ and $\sin^2\theta_{13}$ from three-flavor neutrino oscillation analyses with various combinations of experimental data. These results come from the latest KamLAND data-release [8] in 2013.

Data combination	Δm^2_{21}	$\tan^2\theta_{12}$	$\sin^2\theta_{13}$
KamLAND	$7.54^{+0.19}_{-0.18}$	$0.481^{+0.092}_{-0.080}$	$0.010^{+0.033}_{-0.034}$
KamLAND + solar	$7.53^{+0.19}_{-0.18}$	$0.437^{+0.029}_{-0.026}$	$0.023^{+0.015}_{-0.015}$
KamLAND + solar + θ_{13}	$7.53^{+0.18}_{-0.18}$	$0.436^{+0.029}_{-0.025}$	$0.023^{+0.002}_{-0.002}$

weighted average reactor baseline. The oscillatory shape of the signal is clear, arising from the $\sin^2\left(1.27\frac{\Delta m^2_{12}L}{E}\right)$ term in the $\bar{\nu}_e$ survival probability expression. The shape is somewhat distorted due to multiple reactor baselines and the fact that $\bar{\nu}_e$'s are emitted in a spectrum of energies.

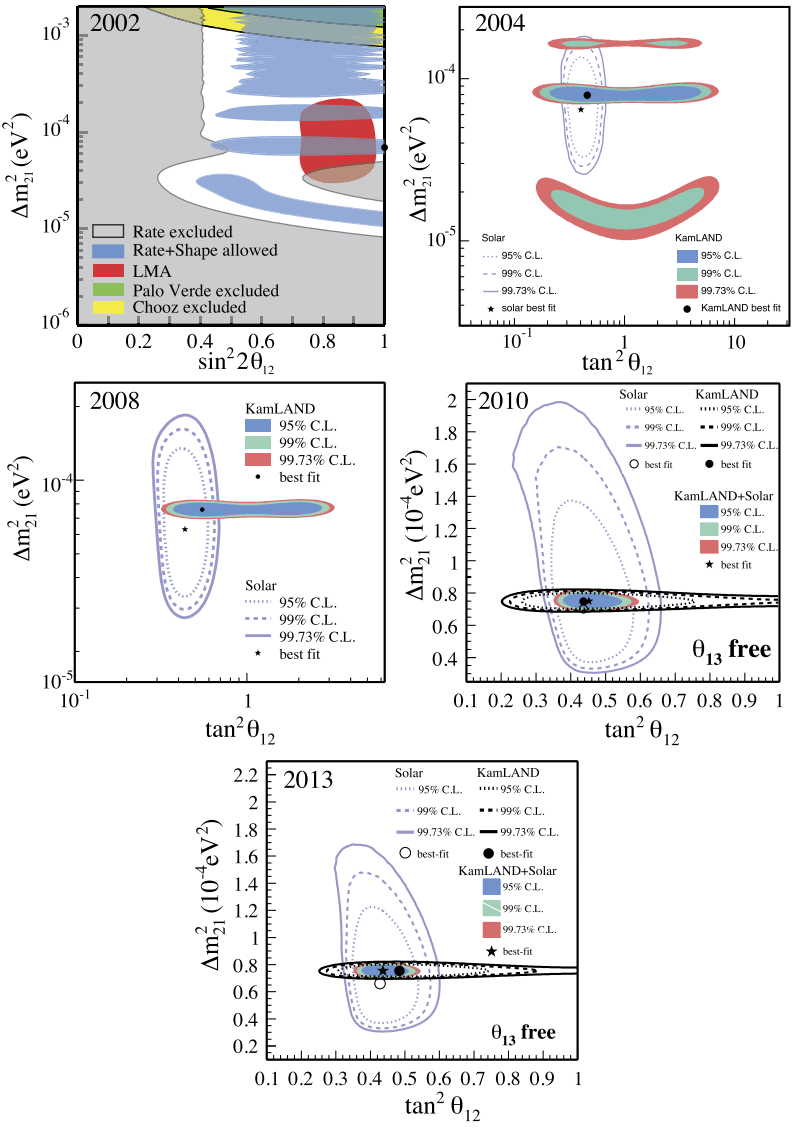

Fig. 5. Allowed neutrino oscillation parameter regions from KamLAND and solar neutrino experiments for the different KamLAND data-releases (the data-release year is shown in the upper left corner of each panel). Each successive data release allowed a more precise determination of the oscillation parameters. While the KamLAND analysis up to 2010 was usually carried out in the 2-ν framework, the high precision data available in 2010 and 2013 allowed placing constraints on the θ_{13} parameter. Figures adapted from [4–8]. (For interpretation of the references to color in this figure, the reader is referred to the web version of this article.)

5.2. *Other results*

While the primary focus of the KamLAND experiment has been the search for, and precision measurement of, neutrino oscillation effects, the experiment has also provided a number of other important measurements. The KamLAND Collaboration performed the first experimental study

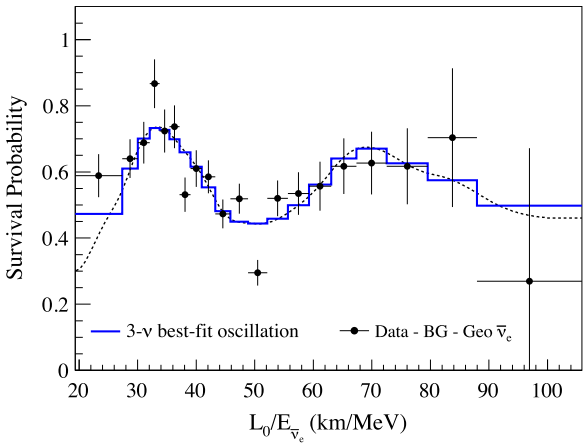

Fig. 6. Illustration of the neutrino oscillation effect. The ratio of the observed $\bar{\nu}_e$ spectrum to the expectation for no-oscillation as a function of $L_0/E_{\bar{\nu}_e}$ is shown for the KamLAND data. $L_0 = 180$ km is the effective flux-weighted average reactor baseline. The histogram and curve show the expectation accounting for the distances to the individual reactors and time-dependent $\bar{\nu}_e$ flux variations and includes the 3-ν best-fit oscillation parameters listed on the last line of Table 1.

of geo-neutrinos [17], significantly improving the results later [18,8]. The collaboration studied astrophysical sources of neutrinos such as solar-^{7}Be [20] and ^{8}B [21], and extraterrestrial antineutrino sources [12,22]. The experiment has also been used to set limits on the invisible decay of neutrons [23] and proton decay [24].

6. Conclusions

The KamLAND experiment has been operational since the beginning of 2002. The experiment has monitored the $\bar{\nu}_e$ flux from more than 50 Japanese nuclear reactors over more than a decade. The KamLAND results have allowed to establish the LMA-MSW neutrino oscillation mechanism as the solution to the solar neutrino flavor transformation. The large collection of reactor $\bar{\nu}_e$ events coming from an average baseline of 180 km enable a precise determination of the Δm^2_{21} neutrino oscillation parameter.

Although the KamLAND detector has been modified to study neutrinoless double beta decay in ^{136}Xe in September 2011, the experiment also continues to be used to monitor reactor antineutrinos and other sources of (anti-)neutrinos.

Acknowledgements

The KamLAND experiment is supported by JSPS KAKENHI Grants No. 16002002 and No. 21000001; the World Premier International Research Center Initiative (WPI Initiative), MEXT, Japan; Stichting FOM in the Netherlands; and under the U.S. Department of Energy (DOE) Grants No. DE-AC02-05CH11231 and No. DE-FG02-01ER41166, as well as other DOE and NSF grants to individual institutions. The Kamioka Mining and Smelting Company has provided service for activities in the mine.

References

[1] A. Suzuki, Present status of KamLand, Nucl. Phys. B, Proc. Suppl. 77 (1–3) (1999) 171–176, http://dx.doi.org/10.1016/S0920-5632(99)00414-4, URL http://www.sciencedirect.com/science/article/pii/S0920563299004144.

[2] A. Suzuki, Antineutrino science in KamLAND, Eur. Phys. J. C 74 (10) (2014) 3094, http://dx.doi.org/10.1140/epjc/s10052-014-3094-x, arXiv:1409.4515.

[3] K.S. Hirata, et al., Observation in the Kamiokande-II detector of the neutrino burst from supernova SN1987A, Phys. Rev. D 38 (1988) 448–458, http://dx.doi.org/10.1103/PhysRevD.38.448.

[4] K. Eguchi, et al., First results from KamLAND: evidence for reactor anti-neutrino disappearance, Phys. Rev. Lett. 90 (2003) 021802, http://dx.doi.org/10.1103/PhysRevLett.90.021802, arXiv:hep-ex/0212021.

[5] T. Araki, et al., Measurement of neutrino oscillation with KamLAND: evidence of spectral distortion, Phys. Rev. Lett. 94 (2005) 081801, http://dx.doi.org/10.1103/PhysRevLett.94.081801, arXiv:hep-ex/0406035.

[6] S. Abe, et al., Precision measurement of neutrino oscillation parameters with KamLAND, Phys. Rev. Lett. 100 (2008) 221803, http://dx.doi.org/10.1103/PhysRevLett.100.221803, arXiv:0801.4589.

[7] A. Gando, et al., Constraints on θ_{13} from a three-flavor oscillation analysis of reactor antineutrinos at KamLAND, Phys. Rev. D 83 (2011) 052002, http://dx.doi.org/10.1103/PhysRevD.83.052002, arXiv:1009.4771.

[8] A. Gando, et al., Reactor on–off antineutrino measurement with KamLAND, Phys. Rev. D 88 (3) (2013) 033001, http://dx.doi.org/10.1103/PhysRevD.88.033001, arXiv:1303.4667.

[9] S. Abe, et al., Production of radioactive isotopes through cosmic muon spallation in KamLAND, Phys. Rev. C 81 (2010) 025807, http://dx.doi.org/10.1103/PhysRevC.81.025807, arXiv:0907.0066.

[10] T.I. Banks, et al., A compact ultra-clean system for deploying radioactive sources inside the KamLAND detector, Nucl. Instrum. Methods A 769 (2014) 88–96, http://dx.doi.org/10.1016/j.nima.2014.09.068, arXiv:1407.0413.

[11] B.E. Berger, et al., The KamLAND full-volume calibration system, J. Instrum. 4 (2009) P04017, http://dx.doi.org/10.1088/1748-0221/4/04/P04017, arXiv:0903.0441.

[12] K. Eguchi, et al., A high sensitivity search for anti-nu(e)'s from the sun and other sources at KamLAND, Phys. Rev. Lett. 92 (2004) 071301, http://dx.doi.org/10.1103/PhysRevLett.92.071301, arXiv:hep-ex/0310047.

[13] A. Gando, et al., Measurement of the double-β decay half-life of ^{136}Xe with the KamLAND-Zen experiment, Phys. Rev. C 85 (2012) 045504, http://dx.doi.org/10.1103/PhysRevC.85.045504, arXiv:1201.4664.

[14] K. Nakajima, K. Inoue, K. Owada, F. Suekane, A. Suzuki, G. Hirano, S. Kosaka, T. Ohta, H. Tanaka, A simple model of reactor cores for reactor neutrino flux calculations for the KamLAND experiment, Nucl. Instrum. Methods A 569 (2006) 837–844, http://dx.doi.org/10.1016/j.nima.2006.09.088, arXiv:physics/0607126.

[15] K. Schreckenbach, G. Colvin, W. Gelletly, F. Von Feilitzsch, Determination of the anti-neutrino spectrum from U-235 thermal neutron fission products up to 9.5-MeV, Phys. Lett. B 160 (1985) 325–330, http://dx.doi.org/10.1016/0370-2693(85)91337-1.

[16] A.A. Hahn, K. Schreckenbach, G. Colvin, B. Krusche, W. Gelletly, F. Von Feilitzsch, Anti-neutrino spectra from ^{241}Pu and ^{239}Pu thermal neutron fission products, Phys. Lett. B 218 (1989) 365–368, http://dx.doi.org/10.1016/0370-2693(89)91598-0.

[17] T. Araki, et al., Experimental investigation of geologically produced antineutrinos with KamLAND, Nature 436 (2005) 499–503, http://dx.doi.org/10.1038/nature03980.

[18] A. Gando, et al., Partial radiogenic heat model for Earth revealed by geoneutrino measurements, Nat. Geosci. 4 (2011) 647–651, http://dx.doi.org/10.1038/ngeo1205.

[19] Q.R. Ahmad, et al., Direct evidence for neutrino flavor transformation from neutral current interactions in the Sudbury Neutrino Observatory, Phys. Rev. Lett. 89 (2002) 011301, http://dx.doi.org/10.1103/PhysRevLett.89.011301, arXiv:nucl-ex/0204008.

[20] A. Gando, et al., ^{7}Be solar neutrino measurement with KamLAND, Phys. Rev. C 92 (5) (2015) 055808, http://dx.doi.org/10.1103/PhysRevC.92.055808, arXiv:1405.6190.

[21] S. Abe, et al., Measurement of the ^{8}B solar neutrino flux with the KamLAND liquid scintillator detector, Phys. Rev. C 84 (2011) 035804, http://dx.doi.org/10.1103/PhysRevC.84.035804, arXiv:1106.0861.

[22] A. Gando, et al., A study of extraterrestrial antineutrino sources with the KamLAND detector, Astrophys. J. 745 (2012) 193, http://dx.doi.org/10.1088/0004-637X/745/2/193, arXiv:1105.3516.

[23] T. Araki, et al., Search for the invisible decay of neutrons with KamLAND, Phys. Rev. Lett. 96 (2006) 101802, http://dx.doi.org/10.1103/PhysRevLett.96.101802, arXiv:hep-ex/0512059.

[24] K. Asakura, et al., Search for the proton decay mode $p \to \bar{\nu} K^{+}$ with KamLAND, Phys. Rev. D 92 (5) (2015) 052006, http://dx.doi.org/10.1103/PhysRevD.92.052006, arXiv:1505.03612.